AIMS Materials Science, 9(4): 554–571.
DOI: 10.3934/matersci.2022033
Received: 15 February 2022
Revised: 14 May 2022
Accepted: 10 June 2022
Published: 15 July 2022

http://www.aimspress.com/journal/Materials

Research article

Influence of laser processing conditions for the manufacture of microchannels on ultrahigh molecular weight polyethylene coated with PDMS and PAA

Eko Sasmito Hadi[1,2,*], Ojo Kurdi[2], Ari Wibawa BS[1], Rifky Ismail[2] and Mohammad Tauviqirrahman[2]

[1] Department Naval Architecture, Faculty of Technology, Diponegoro University, Jl. Prof Sudharto, Tembalang, Semarang, Central Java 50275, Indonesia
[2] Department Mechanical Engineering, Faculty of Technology, Diponegoro University, Jl. Prof Sudharto, Tembalang, Semarang, Central Java 50275, Indonesia

* **Correspondence:** Email: ekosasmito@ft.undip.ac.id; Tel: +62-819-012-80458; Fax: +62-24-76480764.

Abstract: Ultrahigh molecular weight polyethene (UHMWPE) is employed as a bearing material in a range of applications due to its improved elasticity, compatibility, and impact resistance, processing conditions for a suitable surface texture are necessary. Surface texture processing on microchannels using lasers is always associated with the effect of heat damage on the polymer specimen surface. This study aims to explore the use of polydimethylsiloxane (PDMS) and polyacrylic acid (PAA) in the form of liquid gel coatings in order to reduce heat damage to surfaces during the laser processing of ultrahigh molecular weight polyethene (UHMWPE). First, PDMS and PAA were coated on the surface of the UHMWPE material specimen, and then texturing was performed using a laser diode and cleaned using the ultrasonic method. Second, the dimensions and texture profiles of all the samples from this study were measured using a confocal microscope and open source software. In addition, the effect of adding liquid gel on the surface at 150 μm thickness and laser power parameters was determined. The results show that the PDMS and PAA liquid gel layers help regulate the dimensional bulge of the fabricated microchannels at laser powers below 6 watts, compared to those produced without the coating.

Keywords: laser surface texturing; heat damage; surface texturing; coated; confocal microscope; liquid gel; laser diode

1. Introduction

Ultrahigh molecular weight polyethylene (UHMWPE) is a widely used polymer in engineering applications because of its many functional properties, including its high wear resistance, self-lubrication, high impact resistance, and chemical inertia [1]. It also has low water absorption and friction properties [2]. Therefore, UHMWPE is also used in many industrial applications, such as water-lubricated bearings [3] and bearing bushings [4]. However, there are still some problems when using UHMWPE as seawater lubricating bearings used in modern ships, namely, the frictional speed limit is still relatively low [5], and the influence of solid objects dissolved in the lubricating media causes the wear performance to decrease [6].

Several researchers have devised a variety of strategies for increasing UHMWPE wear resistance, including mixing pure materials with appropriate fillers, such as nano-diamond [7], crystallinity [8], cross-linking [9], and the application of texturing on friction surfaces [10]. Producing a variety of textures on the surface of UHMWPE can reduce the polymer contact surface temperature and the friction coefficient [11]. The presence of well-defined and precise textures minimises the contact area, and the load is divided equally between the pressure of the fluid film and the asperity contact. The lubricant medium trapped in the surface also provides space for a different medium [10]. Several texture-making techniques based on various processes, such as microindentation [12], electroerosion [13], and textured lasers [14], have been developed. Among these processes, laser surface texturing (LST) has received considerable attention because of its unique advantages, including rapid processing, high efficiency, excellent control, environmental friendliness, and the ability to create surface textures with increased complexity and accuracy [15].

Several studies have sought to determine the influence of textures on the tribological performance of UHMWPE. Zhang et al. [16] analysed the friction properties of different patterned geometries, including rectangles, circles, and triangles, and found that squares and rectangles provide superior characteristics to rings. However, the creation of textured geometries using laser texturing is challenging because of the high melting viscosity of UHMWPE. Dougherty et al. [10] examined the influence of variations in the lubrication regime and load speed on reducing the friction coefficient of UHMWPE. A 50% reduction in the friction resistance of textured UHMWPE (vs. untextured UHMWPE) was obtained as the lubrication regime shifted from boundary to mixed to full lubrication. Riveiro et al. [17] found that adding dimple textures to the surface of the UHMWPE material improved its tribological performance, with textured UHMWPE beating untextured UHMWPE in a wear test under different loading conditions.

Several researchers have concentrated on using a laser to create surface textures on polymer materials. Riveiro et al. [17] studied the effects of some laser texturing conditions, such as the scanning speed, pulse frequency, place overlap, and irradiance, on controlling the melt viscosity and changing the cell-material interactions of UHMWPE. Previous researchers [18] used a carbon-plated UHMWPE sample and laser processing to produce textures on the polymer surface with specific dimensions. Also, the influences under different conditions were studied, such as at room temperature, at freezing temperatures by having an ice layer, using distilled water, and using

aluminium foil with varying laser processing parameters, including scanning speed, pulse frequency, and laser intensity. The group found that producing a layer of distilled water on the UHMWPE disk does not help create required textures. Textures with specific dimensions could be manufactured using aluminium foil plating. However, details of the dimensions and morphology of the sample surface were not described. The researchers [19] investigated laser ablation on PMMA covered with 2 mm layers of water, ethanol, and air. This work discussed the depth, width, aspect ratio, and HAZ obtained, but did not discuss the occurrence of bulging. In addition, researched the laser ablation of PMMA with a coating of kraft tape or a microfluidic device and discussed the influence of laser power and scanning speed on the resulting groove width and depth [20]. However, this work did not address the issue of bulging.

Numerous researchers have focused on applying lasers to the creation of textures on polymer materials. However, even though water, ethanol, kraft tape, and aluminium foil have been utilised to obtain the required forms, the heat damage impact induced by the laser has yet to be fully addressed. Furthermore, to the best of our knowledge, there is no literature on precisely controlling and practically melting viscosity to create textures with specific dimensions. The process parameters heavily influence direct laser texturing of the material surface, such as laser power, scan speed, beam point size, and the number of passes. In general, the groove depth and width increase with increasing laser power for a given laser point size. Therefore, it is essential to cover or coat the surface of UHMWPE with a more flame retardant material to prevent heat damage and achieve a more acceptable shape. Here we present a study investigating the use of the UHMWPE surface coating method using a liquid gel with flame retardant and flame retardant properties to achieve the desired texture on polymer surfaces via laser processing. The liquid gel layers used were PDMS and PAA. The PDMS gel material has the characteristics of high flexibility [21], excellent electrical insulation [22], and heat resistance to temperatures exceeding 250 ℃ [23].

On the other hand, PAA is frequently utilised as a multifunctional addition for intumescent-based and flame-retardant coatings [24]. It also has a low heat release capability when compared to other polymer materials, including certain refractory ones [25]. This work investigates the use of PDMS and PAA as protective surface coatings for UHMWPE in laser surface texture processing, the texture quality, depth, and width of the texture grooves generated by the laser on the surface of the UHMWPE were investigated.

2. Materials and methods

A UHMWPE (Henan Sanyou Plastic Engineering Development Co., Ltd) with a thickness of 5 mm and a density of 1000 kg/m^3 was used in this research. The dimensions and properties of the UHMWPE specimen are given in Tables 1 and 2. A black sample was chosen because it absorbs elasticity well and is easy to see when being analyzed.

Table 1. Physical properties of the specimen.

Property	Value
Width	5 mm
Length	10 mm
Thickness	5 mm
Colour	Black
Surface roughness	0.2–0.25 ± 0.04 μm

Table 2. Physical properties of the UHMWPE [26].

Property	Value
Melting temperature (°C)	132–138
Molecular weight (10^6 g/mol)	3.5–7.5
Specific gravity	0.925–0.945
Poisson's ratio	0.46
Modulus of elasticity (GPa)	0.5–0.8
Tensile ultimate strength (MPa)	39–48
Tensile yield strength (MPa)	21–28
Tensile ultimate elongation (%)	350–525
Degree of crystallinity (%)	39–75
Impact strength (J/m of notch)	1070
Wear rate ($mm^6/10^6$ cycles)	80–100

The liquid gel material PDMS (Zaoyang Jinpeng Chemical Co., Ltd:–Index Item 201-20) is distinguished by its great flexibility [21], superior electrical insulation [22], and resilience to temperatures above 250 ℃ [23]. In addition, PDMS has transparent optical properties, is inert, nontoxic, flexible, biocompatible, and non-flammable [24]. The PDMS properties are summarised in Table 3.

Table 3. Physical properties of PDMS polymers [25, 27].

Property	Value
Mass density	0.97 kg/m^3
Poisson ratio	0.5
Specific heat	1.46 kJ/kg·K
Thermal conductivity	0.15 W/m·K
Relative dielectric constant	2.3–2.8
Index of refraction	1.4
Electrical resistivity	4×10^{13} Ω·m
Magnetic permeability	0.6×10^6 cm^3/g
Boiling point	155–220 ℃
Melting point	~−40 ℃

PAA (Zhengzhou Meiya Chemical Products Co., Ltd: CAS NO. 9003-01-4) is often used as a multifunctional additive for intumescent-based and flame-retardant coatings [28]. PAA also has a low

heat release capacity comparable with that of other polymer materials, including some that are flame retardant [29]. In addition, PAA has a high thermal conductivity (approaching 0.4 W/m·K), which appears between the polymer chains with the ability to form hydrogen bonds. Since hydrogen bonds are substantially more robust than the conventional van der Waals interactions between polymer chains, the results are consistent with increased heat transfer due to strengthened intermolecular connections [30]. The properties of PAA are summarised in Table 4.

Table 4. Physical properties of the PAA polymer [27,30,31].

Property	Value
Density	1.09 (30% aq.)
Boiling point	116 ℃
Melting point	106 ℃
Thermal conductivity	0.37 W/m·K
Molecular formula	$(C_3H_4O_2)n$
Molecular weight	72.06270
Flash point	61.6 ℃
Exact mass	72.02110
PSA	37.30000
LogP	0.25700
Index of refraction n20/D	1.442

A custom diode laser system was used to manufacture microchannels on the polymer substrate. This laser system includes a laser head diode (OPT-A-B20000, Sharp Corp., Japan), a two-step motor (35HSH24140-18, Sanyo Denki Electric Co., Ltd., Japan), a microcontroller (Arduino Uno Rev 3, Arduino, Italy), and two steel rails. The wavelength of the laser diode used in this study was 520 nm. Another structural component of the proposed laser system enabled cutting of the UHMWPE plate (thickness, 8 mm). The system output power could be adjusted from 0 to 20 W, and the laser head could move in the X and Y directions with scan speeds ranging from 0 to 70 mm/s.

The process of creating a microchannel on UHMWPE is shown in Figure 1. First, the UHMWPE specimen (Figure 1a) was coated with a 150 μm-thick PDMS and PAA layer via screen printing (Figure 1b). Begin by placing a screen 3 mm above the surface of the UHMWPE. A liquid gel is placed at the top of the screen, and a squeeze is used to push the liquid gel through the holes in the screen. With a slight downward force, move the squeegee to another part of the screen. This effectively fills the gauze holes in the screen with liquid gel. The liquid gel in the screen opening seems to be forced by capillary action onto the UHMWPE surface in a certain amount, which is in the form of liquid gel deposits proportional to the thickness and size of the screen. When the squeegee moves to the other side of the screen, the screen tension will pull the screen away from the UHMWPE surface, leaving a liquid gel on the UHMWPE surface. This method was discussed by Wang et al. [32]. The American Society for Testing and Materials (ASTM) D1212-91 [33] was used to measure the surface coating. Second, polymer sheets coated with the liquid gels were engraved using a laser diode (Figure 1c) with the parameters shown in Table 5. Third, the etched UHMWPE substrate was washed with distilled water in an ultrasonic cleaning machine for 10 minutes to remove the liquid gel and ablated materials (Figure 1d). The results of the UHMWPE engraving by diode laser (Figure 1e) were visualised using a trinocular metallurgical material science industrial

instrument equipped with a 34 MP camera (ME300TZB-2L-9M, AmScope-United Scope, Canada) and evaluated using Gwydion (http://gwyddion.net/) [34] and ImageJ (https://imagej.nih.gov/ij/) [35] software.

Table 5. Parameters used in the experiment.

Process parameter	Value
Laser average power (W)	1, 2, 3, 4, 5, 6, 7, 8
Laser pulse duration (ns)	130
Laser pulse frequency (kHz)	20
Laser traverse speed (mm/s)	10
Processing environment	Air, PDMS liquid gel, PAA liquid gel
Liquid gel thickness (μm)	150

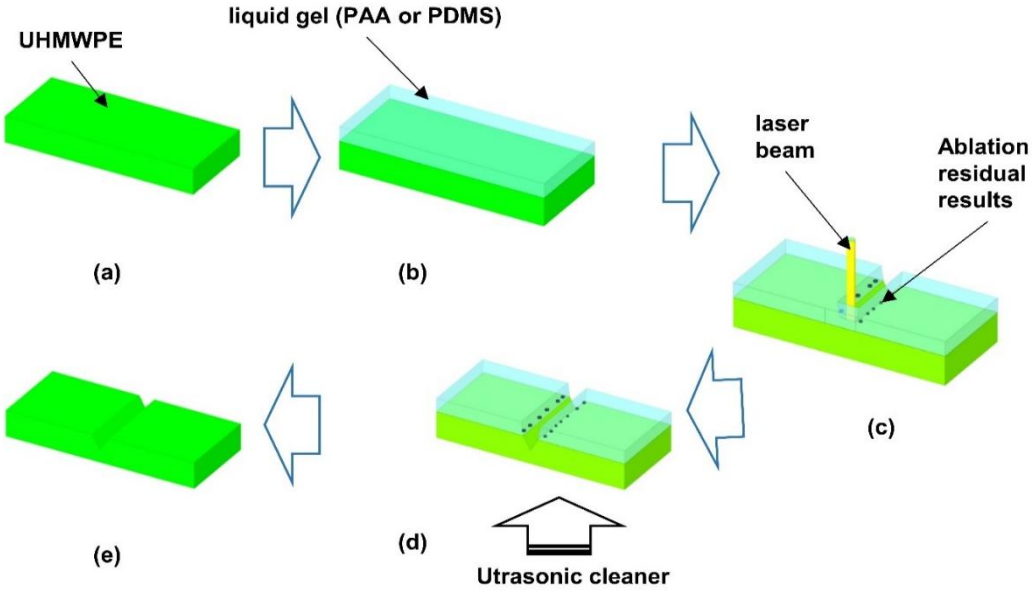

Figure 1. Schematic of the experimental procedure: (a) Specimens are cut to size following Table 1; (b) PDMS or PAA-coated specimen; (c) A laser diode was used to engrave the liquid gel-coated sample using the parameters listed in Table 5; (d) The ultrasonic approach was used to clean the engraved specimen; (e) The model is now ready for confocal microscope examination.

A collimated laser beam passing through the focusing lens of the laser system used in this work obtains a focused laser beam diameter of 12.6 μm in air. The laser beam must travel through a liquid gel layer in the case of ablation in PDMS and PAA. Thus, the beam's diameter on the workpiece surface is altered by refraction, as shown in Figure 2a. According to Snell's law, the diameter of a laser beam on a working surface (d_b) in liquid form can be calculated as follows [36]:

$$d_b = \frac{2lM^2}{\pi \tan\theta_l}\left\{1+\left[\frac{h_l \pi \tan\theta_l \left(D/2F - \tan\theta_l\right)}{lM^2}\right]^2\right\}^{1/2} \quad (1)$$

where l, M, Θ_l, D, F, and h_l are the laser wavelength (520 nm), laser beam quality (2.27), refractive angle of the laser beam in liquid (PDMS, 5.452 °; PAA, 5.292 °), diameter of the collimated laser beam entering the focusing lens (10.2 mm), focal length of the focusing lens (38 mm), and the liquid layer thickness (0.15 mm), respectively. According to Eq 1, the diameters of the laser beam as it passes through the PDMS and PAA liquid gel layers are 14.05 and 14.88 μm, respectively.

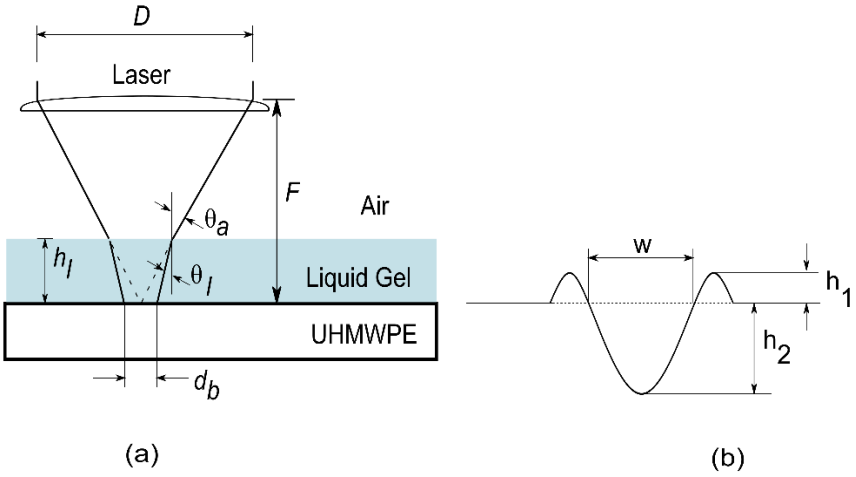

Figure 2. Laser ablation under a liquid layer: (a) refraction of a laser beam in a liquid gel layer, and (b) measurements of the groove geometries.

Thermal damage and melting ejection of materials from the surface are detected when the laser comes into contact with the workpiece's surface. Mannion et al. [37] wrote about the laser intensity threshold for material removal (I_n) in the following way:

$$I_n = I_0 \exp\left(-\frac{2W^2}{d_b^2}\right) \quad (2)$$

where I_n, I_0, W, and d_b are the laser intensity for material removal, the laser beam intensity, the observed groove width, and the laser beam diameter, respectively. The Tangwarodomnukun and Chen [19] and Furziko [38] methods may be used to estimate the groove width (W) of the microchannel formed on the specimen's surface, as shown in Figure 2b, as follows:

$$W = \sqrt{\frac{d_b^2}{2}\left[\ln\frac{l_0}{l_n}\right]^{1/\beta}} \quad (3)$$

where β is an empirical coefficient added to the model to adopt effects that were not considered,

including the plasma protective effect, the reflection of laser beams in the truncated channel, the backpressure, and evaporation dynamics, where the coefficient β is applied to the logarithmic function of the laser intensity ratio resulting from Eq 2. The groove depth (h_2) can be estimated using the method of Tangwarodomnukun and Chen [19] as follows:

$$h_2 = \left[\gamma \frac{l}{\sqrt{n}} \left(\frac{1}{\alpha} + \sqrt{\frac{4\kappa d_b}{\upsilon}} \right) \right]^{1/2} \left[\ln \frac{l_0}{l_n} \right]^{1/\beta} \quad (4)$$

where γ, l, n, α, κ, and v are another empirical coefficient, the laser wavelength (520 nm), the refractive index of the work material (1.528), the absorption coefficient of the work material (562 cm^{-1}) [39] the thermal diffusivity of the work material (1.223×10^{-7} m^2/s) [40] and the laser speed (10 mm/s), respectively. Coefficient γ is added to Eq 4 because this coefficient is related to the level of laser absorption and plasma formation in different media, which varies according to the depth of laser beam penetration.

Each test measurement was obtained five times to meet the statistical analysis requirements with a 95% confidence level, the laser power was increased by 1 Watt, and an analysis of variance (ANOVA) was performed. ANOVA was applied to determine the significance of the laser power parameters and ablation environment on the groove width, groove depth, and bulge formation.

3. Results and discussion

The general laser ablation process is the same across many lasers machining applications, including laser beam milling, high-precision drilling, and laser cutting. Ablation is a mix of evaporation and melt release processes. Electrons on the substrate are activated by laser photons when a focused beam of laser light strikes the specimen surface [41], as shown in Figure 3a. As predicted by Beer-Lambert's law [41,42], this excitation generates heat by absorbing photon energy. Beer Lambert's law says that the amount of light absorbed depends on how thick the material is and how bright the light source is. The heating action causes the material to melt or evaporate, resulting in a loss of macroscopic material from the substrate. Plasma clumps arise as a result of the transition from solid to gas. A variety of mechanisms accomplish this phase change. The initial heat produced by laser photon absorption causes the creation of a melt pool in the laser substrate contact zone. As the pulse penetrates, the temperature rises, and the melt pool evaporates [43]. The molten material is then pushed from the pool, from which it is expelled by the high pressure developed during evaporation, commonly known as the recoil pressure [44], as shown in Figure 3b. The ejected material is a source of concern because of redeposition on the substrate or contact zone [45,46]. The liquid can undergo an explosive liquid-vapour phase transition if the temperature in the laser-substrate interaction zone is raised further [47,48]. The fluid phase dynamics and vapour conditions in this process are highly complicated, and the resolidification of the liquid material leads to a geometric change in the ablation features. As shown in Figure 3c, the surface of the specimen coated with a liquid gel has a heat-absorbing effect that reduces melting or evaporation of the material, preventing the removal of macroscopic material from the substrate and reducing the formation of plasma clumps. The recoil pressure that occurs is not strong enough to push the liquid material out of the pool (Figure 3d).

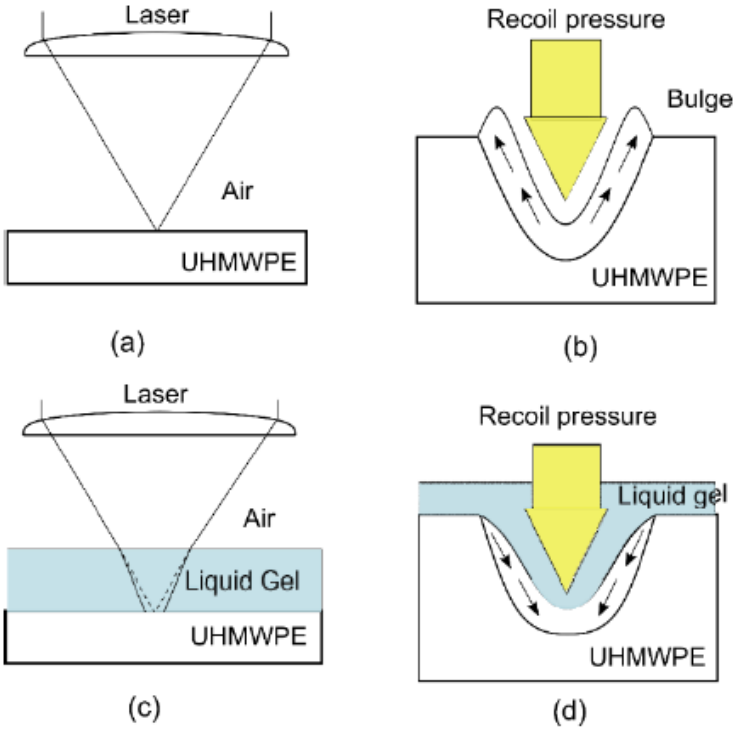

Figure 3. Illustration of the UHMWPE surface using direct laser ablation. (a) without liquid gel; (b) molten material is pushed from the pool by the recoil pressure; (c) with liquid gel; (d) The recoil pressure is not powerful enough to make the liquid material out of the pool.

Figure 4 shows the surface of an uncoated UHMWPE specimen after being subjected to a laser beam with a power of 4 Watts and a transverse speed of 10 mm/s. The confocal microscope acquisition result is shown in Figure 4a, which indicates that the UHMWPE surface has bulges caused by the ablation process at the margins of the created microchannel. Figure 4b,c show the produced microchannels' 3D surface topography and dimensional characteristics.

Each UHMWPE specimen was coated with PAA or PDMS with a thickness of 150 μm, as shown in Figures 5 and 6, and almost no significant bulge was generated. Moreover, the initial heat reduction by the liquid gel layer caused by the absorption of laser photons by the substrate results in the production of a relatively small melt pool in the interaction zone of the laser substrate compared to that without the liquid gel layer. These comparisons are represented in Figures 4–6c. The Gaussian distribution is followed by the resulting characteristic dimensional profile [49]. However, as shown in Figure 4c, it starts to enlarge due to the influence of overheating. Because the energy absorption diode laser is evenly distributed in the UHMWPE material, the profile at the bottom of the created microchannel tends to be half-circular. When the ablation process is done, a half-circular profile is left on the bottom of the pool [20].

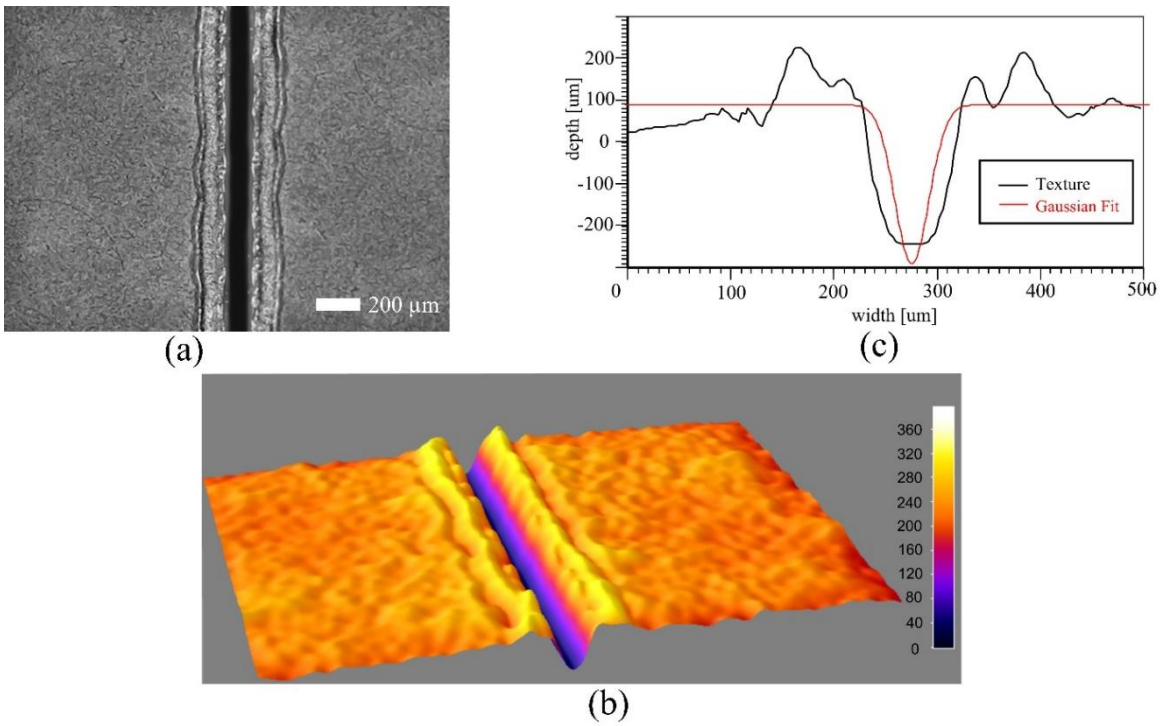

Figure 4. Visualization of the UHMWPE surface using direct laser ablation in air. (a) Acquisition of confocal microscopy, (b) 3D microchannel, (c) microchannel profile.

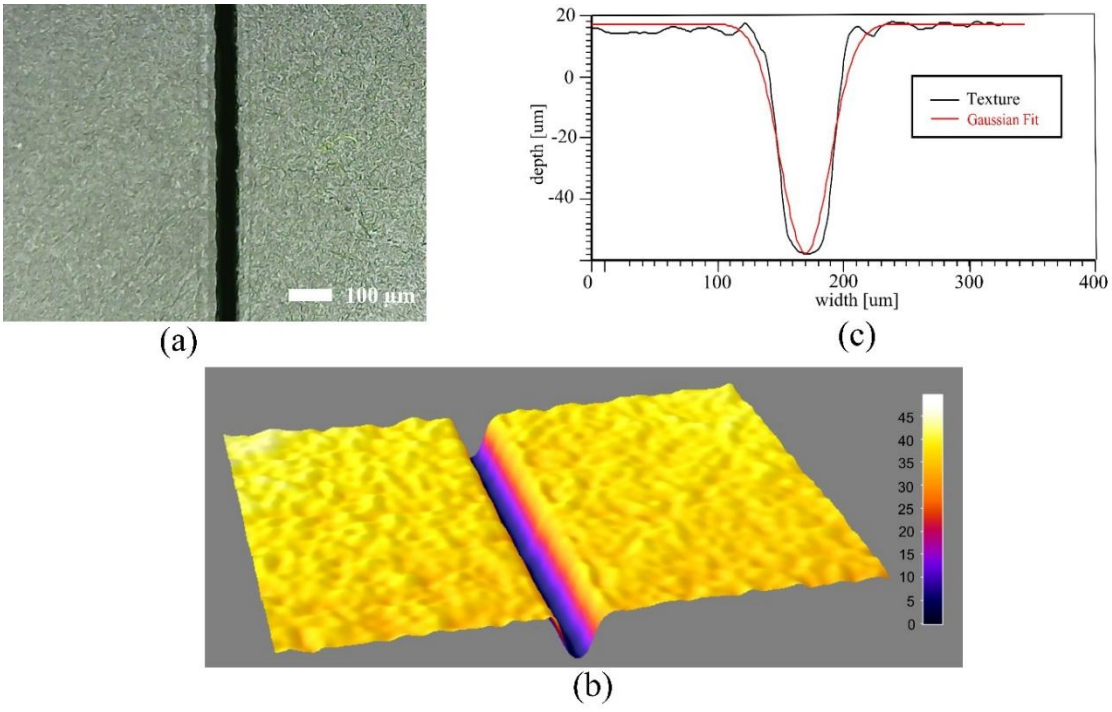

Figure 5. Visualization of the UHMWPE surface using direct laser ablation with PAA coating. (a) Acquisition of confocal microscopy; (b) 3D microchannel; (c) microchannel profile.

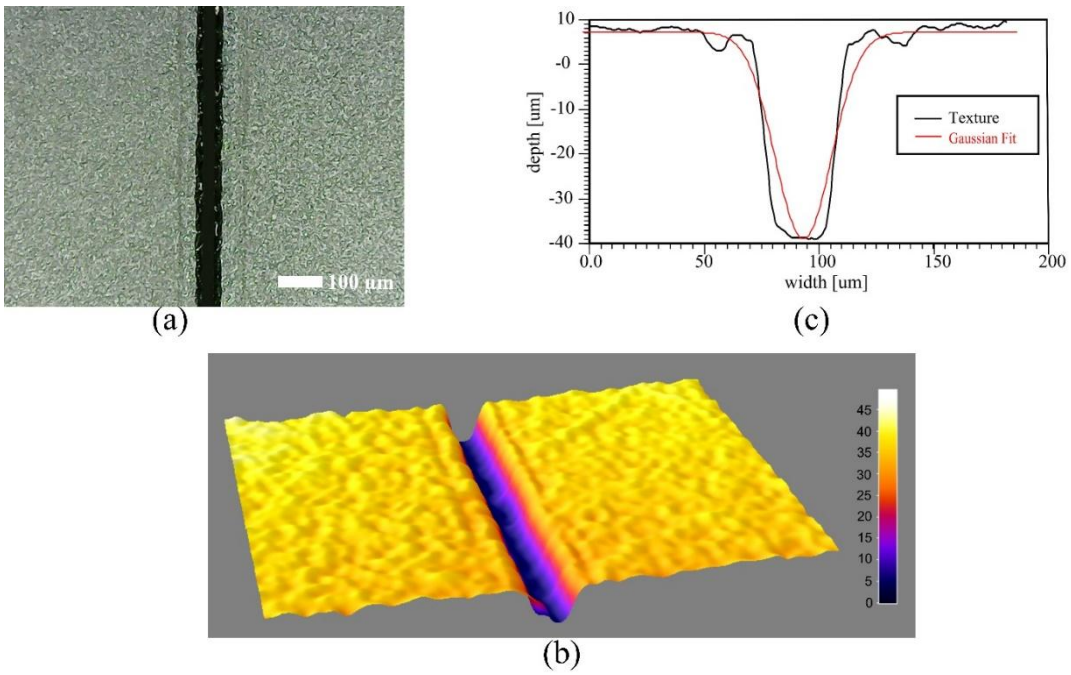

Figure 6. Visualization of the UHMWPE surface using direct laser ablation using PDMS coating. (a) Acquisition of confocal microscopy; (b) 3D microchannel; (c) microchannel profile.

Figure 7a presents the microchannel widths generated by different laser powers in ablation environments. Increasing the laser power can increase the groove width formed on UHMWPE because the high heat of the laser leads to melting and evaporation of the working material in the laser irradiation area and expands the cutting channel. The width of the microchannel produced by air ablation has a roughly linear relationship with laser power. Nevertheless, the width of the liquid gel layer tends to be reduced for laser powers below 6 watts. However, the microchannel widths obtained from ablation in air and the liquid gels are not significantly different at laser powers above 6 W. This finding may be explained by the evaporation of the liquid gel, which reduces the thickness of the liquid coating on the surface of the working material and results in an ablation behavior that is similar to that in air at higher laser powers. The microchannel width obtained during the laser ablation of UHMWPE specimens coated with PDMS liquid gel is smaller than that obtained from ablation in air and PAA liquid gel. Because PDMS can withstand high temperatures [23,50], heat conduction towards the working object material is limited, and the expansion of the microchannel width is inhibited. As a result, the boiling point of PDMS is higher than that of PAA (155–220 ℃ versus 116 ℃), and the former does not evaporate quickly and remains largely on the working surface during ablation. It is also influenced by the optical properties of the liquid gels. Specifically, the bias index of PDMS is lower than that of PAA, and the bias angle of the former (5.452 °) is more significant than that of the latter (5.292 °). The bias angle is therefore proportional to the laser beam (Eq 1). When ablation is done on PDMS, the laser irradiation area and groove width are smaller than when ablation is done on PAA.

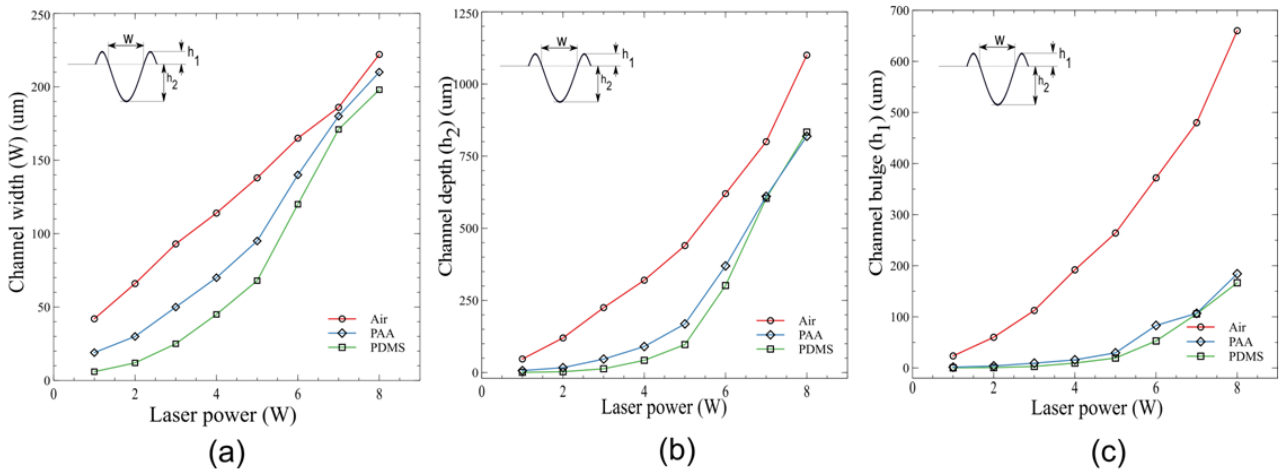

Figure 7. The influence of the laser power and ablation conditions on (a) the channel width, (b) channel depth, and (c) channel bulge.

Figure 7b shows the influence of the average laser power and ablation environment on the groove depth. The results are similar to the previous findings on groove width; i.e., increases in the laser power increase the amount of UHMWPE eliminated, thereby causing broader and deeper grooves. When PDMS and PAA liquid gels are used as cooling media, the depth of the grooves obtained is much shallower than that obtained in air. The high thermal conductivity of the liquid gels (PDMS, 0.15 W/m·K; PAA, 0.37 W/m·K) may be a factor restricting heat penetration into UHMWPE. The liquid gel evaporation rate is relatively low at laser strengths below 6 W, and the liquid gel coating absorbs the laser beam. Such absorption can reduce the intensity of the laser before it reaches the material surface, preventing deeper ablation. Meanwhile, with laser powers greater than 6 watts, the gel layer no longer functions as a cooling medium, and the characteristic of the depth of the microchannel produced is close to the ablation effect in the air.

Figure 7c indicates that the bulge on the surface of the UHMWPE without the PAA and PDMS coatings (i.e., in air) is quite large and tends to have a linear characteristic with increasing laser power. This finding can be explained as follows. As the laser energy increases, the surface of the local material undergoes liquefaction and rapid evaporation. The temperature rises to a certain level because of the incoming energy pulses, and the melt pool reaches evaporation conditions, during which a high pressure develops. This pressure, known as the recoil pressure, drives the liquid material out of the created pond [44]. The recoil pressure then depends on the average laser power density [51]. When the laser energy causing the recoil pressure is significant and the surface tension gradient becomes positive because of the temperature rise, a radial inward flow pushes the liquid material towards the outside. The cooling effect of PDMS and PAA on the liquid surface tension tends to be smaller than the liquid volumetric style and the tilt of the duct wall, resulting in liquid UHMWPE flowing to the base of the channel. Significant bulging does not occur when surfaces coated with PAA are ablated at laser powers below 6 W. When the laser power exceeds 6 W, the temperature gradient causes some liquid gel to evaporate. Zhou et al. [52] also saw this happen, but they did it with different materials.

Figure 8a shows that laser grooving of UHMWPE in air provides the most significant aspect ratio of depth to width or grooves. The aspect ratios obtained on surfaces coated with PDMS and

PAA seem to change slightly when laser powers greater than 6 W are used, likely because of the expansion of the plasma with increasing laser power. When there is significant plasma expansion across the region emitted by the laser, the laser beam cannot efficiently target the workpiece's surface; instead, the laser energy is absorbed by the plasma, and the plasma becomes a heat source. Thermal radiation from plasma can enlarge the groove in any direction, and the aspect ratio of the groove is slightly changed. This ratio consistently increases with the laser power during air ablation because of the absence of the material cooling effect. If the cooling liquid gel reduces the plasma density, most of the laser beam penetrates the workpiece in order to widen the grooves. The laser used may also have greater transparency when applied to the polymer. This property allows diode laser energy absorption to be distributed evenly throughout the material. After occurrence and evaporation, the microchannel forms a half-circular profile. This phenomenon was also observed by Gao et al. [20].

The aspect ratio (h_1/h_2) formed beneath the PDMS and PAA coatings is generally 2.5 times smaller than those obtained without the coating, as shown in Figure 8b. This finding may be explained by the reduction in the recoil pressure in the liquid gel system due to the loss of laser energy through coating adsorption and evaporation of the liquid gel. The liquid gel also prevents heat accumulation by absorbing heat. The liquid gel has a higher heat capacity and thermal conductivity than air, which affects the direction of the liquid polymer flow caused by the surface tension gradient due to the temperature drop. Under almost all of the tested laser powers, the geometric shapes of the bulges made by the liquid gel coatings are smaller than those made in the air.

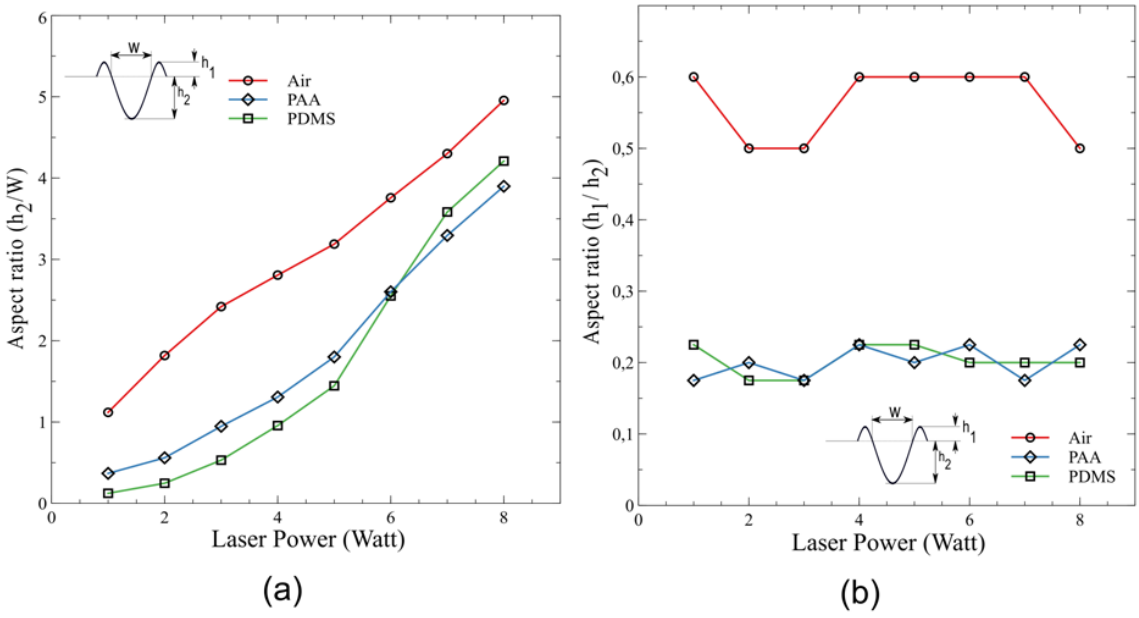

Figure 8. Effect of the laser power and ablation conditions on microchannel aspect ratio profiles. (a) aspect ratio (h_2/W), (b) aspect ratio (h_1/h_2).

After fitting the experimental data to Eqs 3 and 4, the coefficient β and the laser intensity threshold (I_{th}) obtained were 0.21 and 0.0374 mW/cm^2 below the R2 value of 95%. Figure 9a,b show the measured and predicted widths and depths of grooves obtained under various laser intensities and ablation environments. As shown in the figure, the width and depth of the grooves increase with increasing laser intensity. The increasing trend tends to be linear for UHMWPE ablation in air and

appears to conform to a second-order polynomial equation for ablation in liquid gel due to the thermal properties of the PDMS and PAA coatings. However, as the energy intensity of the laser increases and the liquid gel layer begins to evaporate, the results of ablation in the liquid gel environment tend to be identical to those obtained in air. The presence of a liquid gel layer provides thermal conductivity to cool the workpiece during ablation. According to Figure 9a,b, the prediction model results are generally consistent with the experimental results. Differences between the observed and predicted results may be attributed to other nonlinear characteristics of the laser beam and interactions with the workpiece material. Based on the experimental findings, a low laser intensity setting is recommended during UHMWPE ablation to provide the appropriate geometric aspect ratio characteristics while avoiding undesirable shape damage due to heat damage on the surface of the UHMWPE material. High machining performance may be obtained when a liquid gel PDMS and PAA are used to achieve the laser texturing of UHMWPE, resulting in relatively lower groove aspect ratios and bulge sizes than those obtained in an air environment.

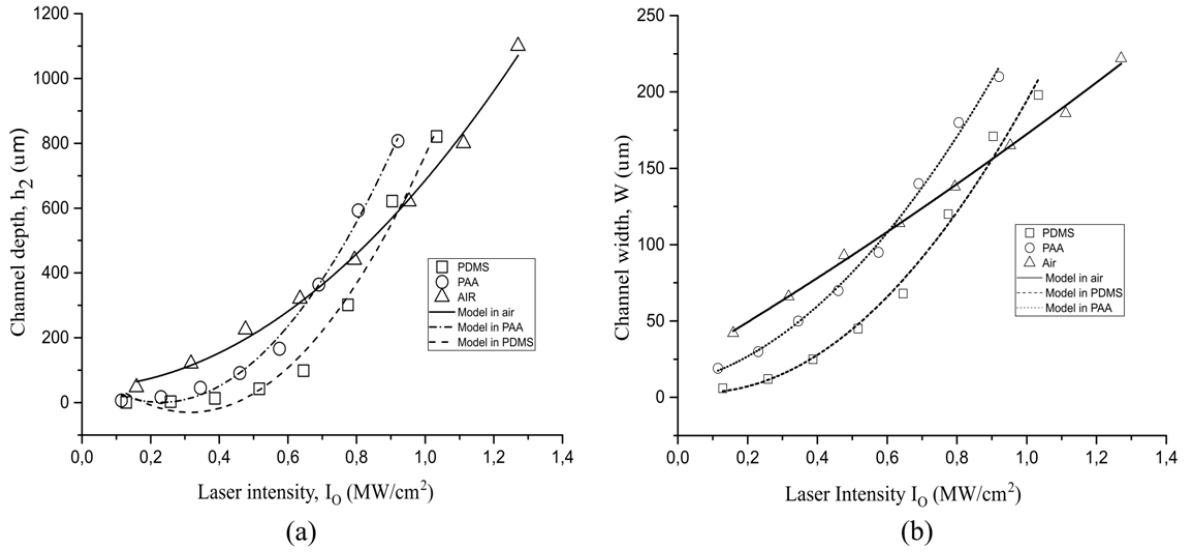

Figure 9. Comparison between the predicted and measured (a) channel depths and (b) channel widths under various laser intensities.

5. Conclusions

The optical and thermal effects of the laser ablation environment on the UHMWPE surface geometry and morphology were examined. Specifically, PDMS and PAA liquid gels were selected as media to promote UHMWPE laser grooving. The experimental findings revealed that the average laser power increases the width, depth, and bulge size. Cleaner surface textures, less deposition, and less thermal damage could be obtained when ablation was performed in a liquid gel environment with a relatively low laser energy intensity. However, at specific laser energy intensities, for example, when the laser energy intensity can vaporise the liquid gel layer, the aspect ratio and bulge size obtained in the liquid gel environment were similar to those obtained from ablation in air. Furthermore, the results of this study are preliminary, so further research is needed to improve UHMWPE microchannels by coating with PDMS or PAA in order to provide significant benefits for

UHMWPE laser processing through surface coating with PDMS and PAA liquid gels and further enhance the laser ablation process on polymeric materials to reduce heat damage in fine-scale industrial manufacturing.

Acknowledgments

The authors acknowledge the Doctoral Program of the Department of Mechanical Engineering, Diponegoro University, Semarang, Indonesia. The authors are sincerely grateful to Dr. Ferry Anggoro Ardy Nugroho (Marie Sklodowska-Curie, Postdoctoral Fellow at Vrije Universiteit Amsterdam) for inspiring and discussing this article.

Conflict of Interest

All authors declare no conflicts of interest in this paper.

References

1. Drakopoulos SX, Psarras GC, Forte G, et al. (2018) Entanglement dynamics in ultra-high molecular weight polyethylene as revealed by dielectric spectroscopy. *Polymer* 150: 35–43. https://doi.org/10.1016/j.polymer.2018.07.021.
2. Golchin A, Simmons GF, Glavatskih S, et al. (2013) Tribological behaviour of polymeric materials in water-lubricated contacts. *P I Mech Eng J-J Eng* 227: 811–825. https://doi.org/10.1177/1350650113476441.
3. Chang T, Yuan C, Guo Z (2019) Tribological behavior of aged UHMWPE under water-lubricated condition. *Tribol Int* 133: 1–11. https://doi.org/10.1016/j.triboint.2018.12.038.
4. Chen S, Li J, Wei L, et al. (2017) Tribological properties of polyimide-modified UHMWPE for bushing materials of seawater lubricated sliding bearings. *Tribol Int* 115: 470–476. https://doi.org/10.1016/j.triboint.2017.06.011.
5. Cho MH, Bahadur S, Pogosian AK (2005) Friction and wear studies using Taguchi method on polyphenylene sulfide filled with a complex mixture of MoS_2, Al_2O_3, and other compounds. *Wear* 258: 1825–1835. https://doi.org/10.1016/j.wear.2004.12.017.
6. Ramadan MA (2018) Friction and wear of sand-contaminated lubricated sliding. *Friction* 6: 457–463. https://doi.org/10.1007/s40544-017-0192-4.
7. Golchin A, Villain A, Emami N (2017) Tribological behaviour of nanodiamond reinforced UHMWPE in water-lubricated contacts. *Tribol Int* 110: 195–200. https://doi.org/10.1016/j.triboint.2017.01.016.
8. Bruck AL, Karuppiah KS, Sundararajan S, et al. (2010) Friction and wear behavior of ultrahigh molecular weight polyethylene as a function of crystallinity in the presence of the phospholipid dipalmitoyl phosphatidylcholine. *J Biomed Mater Res B* 93: 351–358. https://doi.org/10.1002/jbm.b.31587.
9. Atwood SA, Van Citters DW, Patten EW, et al. (2011) Tradeoffs amongst fatigue, wear, and oxidation resistance of cross-linked ultra-high molecular weight polyethylene. *J Mech Behav Biomed Mater* 4: 1033–1045. https://doi.org/10.1016/j.jmbbm.2011.03.012.

10. Dougherty PSM, Srivastava G, Onler R, et al. (2015) Lubrication enhancement for UHMWPE sliding contacts through surface texturing. *Tribol Trans* 58: 79–86. https://doi.org/10.1080/10402004.2014.933935.
11. Kustandi TS, Choo JH, Low HY, et al. (2009) Texturing of UHMWPE surface via NIL for low friction and wear properties. *J Phys D Appl Phys* 43: 015301. https://doi.org/10.1088/0022-3727/43/1/015301.
12. Nakatsuji T, Mori A (2001) The tribological effect of mechanically produced micro-dents by a micro diamond pyramid on medium carbon steel surfaces in rolling-sliding contact. *Meccanica* 36: 663–674. https://doi.org/10.1023/A:1016348803781.
13. Wang X, Adachi K, Otsuka K, et al. (2006) Optimization of the surface texture for silicon carbide sliding in water. *Appl Surf Sci* 253: 1282–1286. https://doi.org/10.1016/j.apsusc.2006.01.076.
14. Etsion I (2004) Improving tribological performance of mechanical components by laser surface texturing. *Tribol Lett* 17: 733–737. https://doi.org/10.1007/s11249-004-8081-1.
15. Etsion I (2005) State of the art in laser surface texturing. *J Tribol* 127: 248–253. https://doi.org/10.1115/1.1828070.
16. Zhang YL, Zhang XG, Matsoukas G (2015) Numerical study of surface texturing for improving tribological properties of ultra-high molecular weight polyethylene. *Biosurface Biotribology* 1: 270–277. https://doi.org/10.1016/j.bsbt.2015.11.003.
17. Riveiro A, Soto R, Del Val J, et al. (2014) Laser surface modification of ultra-high-molecular-weight polyethylene (UHMWPE) for biomedical applications. *Appl Surf Sci* 302: 236–242. https://doi.org/10.1016/j.apsusc.2014.02.130.
18. Hussain M, Sufyan M, Abbas N, et al. (2019) Influence of laser processing conditions for texturing on ultra-high-molecular-weight-polyethylene (UHMWPE) surface. *Case Studies in Thermal Engineering* 14: 100491. https://doi.org/10.1016/j.csite.2019.100491.
19. Tangwarodomnukun V, Chen HY (2015) Laser ablation of PMMA in air, water, and ethanol environments. *Mater Manuf Process* 30: 685–691. https://doi.org/10.1080/10426914.2014.994774.
20. Gao K, Liu J, Fan Y, et al. (2019) Ultra-low-cost fabrication of polymer-based microfluidic devices with diode laser ablation. *Biomed Microdevices* 21: 83. https://doi.org/10.1007/s10544-019-0433-6.
21. Katayama S, Kubo Y, Yamada N (2002) Characterization and mechanical properties of flexible dimethylsiloxane-based inorganic/organic hybrid sheets. *J Am Ceram Soc* 85: 1157–1163. https://doi.org/10.1111/j.1151-2916.2002.tb00238.x.
22. Aoki Y (2012) Electrical treeing characteristics in polydimethylsiloxane-based organic-inorganic hybrid materials. *Mol Cryst Liq Cryst* 568: 186–191. https://doi.org/10.1080/15421406.2012.708841.
23. Aoki Y (2016) Heat-resistant, thermally conductive coating of alumina on metal via electrophoretic deposition with added polydimethylsiloxane-based organic–inorganic hybrid materials. *Polym Bull* 73: 2605–2614. https://doi.org/10.1007/s00289-016-1700-9.
24. Mata A, Fleischman AJ, Roy S (2005) Characterization of polydimethylsiloxane (PDMS) properties for biomedical micro/nanosystems. *Biomed Microdevices* 7: 281–293. https://doi.org/10.1007/s10544-005-6070-2.

25. Torrisi L, Cutroneo M, Torrisi A, et al. (2020) IR ns pulsed laser irradiation of Polydimethylsiloxane in vacuum. *Vacuum* 177: 109361. https://doi.org/10.1016/j.vacuum.2020.109361.
26. Kurtz SM (2016) A primer on UHMWPE, *UHMWPE Biomaterials Handbook*, Amsterdam, Netherlands: William Andrew Publishing, 1–6.
27. Material Property Database (polydimethylsiloxane). Available from: https://www.mit.edu/~6.777/matprops/pdms.htm.
28. Price EJ, Covello J, Tuchler A, et al. (2020) Intumescent, epoxy-based flame-retardant coatings based on poly(acrylic acid) compositions. *ACS Appl Mater Interfaces* 12: 18997–19005. https://doi.org/10.1021/acsami.0c00567.
29. Sonnier R, Otazaghine B, Iftene F, et al. (2016) Predicting the flammability of polymers from their chemical structure: an improved model based on group contributions. *Polymer* 86: 42–55. https://doi.org/10.1016/j.polymer.2016.01.046.
30. Xie X, Li D, Tsai TH, et al. (2016) Thermal conductivity, heat capacity, and elastic constants of water-soluble polymers and polymer blends. *Macromolecules* 49: 972–978. https://doi.org/10.1021/acs.macromol.5b02477.
31. ChemSrc. Polyacrylic Acid. CAS#: 9003-01-4. Available from: https://www.chemsrc.com/en/cas/9003-01-4_453957.html#wuHuaDiv.
32. Wang Y, Li P, Sun Z, et al. (2018) A model of screen reaction force for the 3D additive screen printing. *The Journal of The Textile Institute* 109: 1000–1007. https://doi.org/10.1080/00405000.2017.1397834.
33. ASTM International (2013) Standard test methods for measurement of wet film thickness of organic coatings. ASTM D1212-91. Available from: https://www.astm.org/Standards/D1212.htm.
34. Nečas D, Klapetek P (2012) Gwyddion: an open-source software for SPM data analysis. *Cent Eur J Phys* 10: 181–188. https://doi.org/10.2478/s11534-011-0096-2.
35. Mahmoudzadeh R, Salabati M, Hsu J, et al. (2021) Agreement of optical coherence tomography thickness measurements between Heidelberg Eye Explorer and ImageJ software. *CJO* (In press). https://doi.org/10.1016/j.jcjo.2021.05.018.
36. Duangwas S, Tangwarodomnukun V, Dumkum C (2014) Development of an overflow-assisted underwater laser ablation. *Mater Manuf Process* 29: 1226–1231. https://doi.org/10.1080/10426914.2014.930896.
37. Mannion PT, Magee J, Coyne E, et al. (2004) The effect of damage accumulation behaviour on ablation thresholds and damage morphology in ultrafast laser micro-machining of common metals in air. *Appl Surf Sci* 233: 275–287. https://doi.org/10.1016/j.apsusc.2004.03.229.
38. Furzikov N (1990) Approximate theory of highly absorbing polymer ablation by nanosecond laser pulses. *Appl Phys Lett* 56: 1638–1640. https://doi.org/10.1063/1.103150.
39. Kamal A, Bashir M, Firdous S, et al. (2016) Optical properties of ultra-high molecular weight polyethylene (UHMWPE): a material of choice for total joint applications. *Radiat Phys Chem* 118: 102–106. https://doi.org/10.1016/j.radphyschem.2015.03.012.
40. Nunes dos Santos W, Mummery P, Wallwork A (2005) Thermal diffusivity of polymers by the laser flash technique. *Polym Test* 24: 628–634. https://doi.org/10.1016/j.polymertesting.2005.03.007.

41. Brown MS, Arnold CB (2010) Fundamentals of laser-material interaction and application to multiscale surface modification, In: Sugioka K, Meunier M, Piqué A, *Laser Precision Microfabrication*, Berlin, Heidelberg: Springer Berlin Heidelberg, 91–120.
42. Ahmed N, Darwish S, Alahmari AM (2016) Laser ablation and laser-hybrid ablation processes: a review. *Mater Manuf Process* 31: 1121–1142. https://doi.org/10.1080/10426914.2015.1048359.
43. Von der Linde D, Sokolowski-Tinten K (2000) The physical mechanisms of short-pulse laser ablation. *Appl Surf Sci* 154: 1–10. https://doi.org/10.1016/S0169-4332(99)00440-7.
44. Hoffman J (2015) The effect of recoil pressure in the ablation of polycrystalline graphite by a nanosecond laser pulse. *J Phys D Appl Phys* 48: 235201. https://doi.org/10.1088/0022-3727/48/23/235201.
45. Tangwarodomnukun V, Likhitangsuwat P, Tevinpibanphan O, et al. (2015) Laser ablation of titanium alloy under a thin and flowing water layer. *Int J Mach Tool Manu* 89: 14–28. https://doi.org/10.1016/j.ijmachtools.2014.10.013.
46. Singh S, Argument M, Tsui Y, et al. (2005) Effect of ambient air pressure on debris redeposition during laser ablation of glass. *J Appl Phys* 98: 113520. https://doi.org/10.1063/1.2138800.
47. Miotello A, Kelly R (1999) Laser-induced phase explosion: new physical problems when a condensed phase approaches the thermodynamic critical temperature. *Appl Phys A* 69: S67–S73. https://doi.org/10.1007/s003399900296.
48. Bulgakova N, Bulgakov A (2001) Pulsed laser ablation of solids: transition from normal vaporization to phase explosion. *Appl Phys A* 73: 199–208. https://doi.org/10.1007/s003390000686.
49. Sarma U, Joshi SN (2020) Numerical modelling and simulation of microchannel fabrication on polycarbonate using Laser-Induced Plasma Assisted Ablation (LIPAA). *Optik* 223: 165379. https://doi.org/10.1016/j.ijleo.2020.165379.
50. Aoki Y, Yoshioka K (2014) Preparation and characterization of highly heat-resistant organic–inorganic hybrid materials made from two-component polydimethylsiloxane. *Mol Cryst Liq Cryst* 597: 59–64. https://doi.org/10.1080/15421406.2014.932224.
51. Samant AN, Dahotre NB (2008) Computational predictions in single-dimensional laser machining of alumina. *Int J Mach Tool Manu* 48: 1345–1353. https://doi.org/10.1016/j.ijmachtools.2008.05.004.
52. Zhou J, Shen H, Pan Y, et al. (2016) Experimental study on laser microstructures using long pulse. *Opt Laser Eng* 78: 113–120. https://doi.org/10.1016/j.optlaseng.2015.10.009.

AIMS Press

© 2022 the Author(s), licensee AIMS Press. This is an open access article distributed under the terms of the Creative Commons Attribution License (http://creativecommons.org/licenses/by/4.0)